STRATIGRAPHIC IMPLICATIONS OF METEORIC SPHAEROSIDERITE $\delta^{18}O$ VALUES IN PALEOSOLS OF THE CRETACEOUS (ALBIAN) BOULDER CREEK FORMATION, NE BRITISH COLUMBIA FOOTHILLS, CANADA

DAVID F. UFNAR,[1] LUIS A. GONZÁLEZ,[2] GREG A. LUDVIGSON,[2,3] ROBERT L. BRENNER,[1] AND BRIAN J. WITZKE[3]
[1] *Department of Geoscience, University of Iowa, Iowa City, Iowa 52242-1379, U.S.A.*
[2] *Center for Global and Regional Environmental Research, University of Iowa, Iowa City, Iowa 52242, U.S.A.*
[3] *Iowa Geological Survey Bureau, Iowa City, Iowa 52242, U.S.A.*
e-mail: david-ufnar@uiowa.edu

ABSTRACT: **The MD 80-08 coal exploration core from the Albian Boulder Creek Formation of northeastern British Columbia contains 90 m of alluvial strata that underwent extensive pedogenic modification. Gleyed colors, pedogenic slickensides, clay coatings, mottling, sphaerosiderite, and sedimentary pyrite characterize the paleosols.**

The isotopic compositions of 30 sphaerosiderite-bearing horizons commonly show trends of invariant $\delta^{18}O$ and variable $\delta^{13}C$ values. Equal-area plots of $\delta^{18}O$ vs. $\delta^{13}C$ were used to construct meteoric sphaerosiderite lines (MSLs). The MSLs indicate that meteoric groundwater compositions ranged from approximately −11‰ to −16‰ (SMOW). The sphaerosiderite $\delta^{18}O$ values indicate formation in shallow groundwaters predominantly recharged by local precipitation. The sphaerosiderite isotopic compositions are a proxy record of mid-Cretaceous precipitation, and are useful for quantifying changes in the hydrologic cycle during humid ''greenhouse'' periods.

Micromorphology of a 1.15 meter interval (69.75–68.6 m), with a +1.31‰ increase in the average $\delta^{18}O$ values, records a polygenetic history of paleosol development. The pedocomplex has a four-stage developmental history characterized by: (1) an initial well-drained phase, with wet–dry cycles and relatively low baselevel; (2) erosion, baselevel rise and coarser-grained sedimentation; (3) saturated, reducing soil conditions, high baselevel, with some marine influence on pedogenesis; and (4) meteoric-water-dominated hydromorphic soil conditions, high baselevel, and sphaerosiderite precipitation. The $\delta^{18}O$ excursion recorded through this interval reflects minor mixing of marine and meteoric groundwaters. The modal abundance of pyrite, and increased Mg/(Ca + Mg) and Mg/Fe cation ratios in the sphaerosiderites further substantiate marine influence on pedogenesis.

The alluvial section of the Boulder Creek Formation is aggradational, and several changes in baselevel recorded in the paleosols are interpreted to have been driven by minor (parasequence-scale) changes in relative sea level.

INTRODUCTION

The use of sphaerosiderite $\delta^{18}O$ and $\delta^{13}C$ values as a proxy record for paleoclimatic and paleohydrologic information is a recent development made possible by the recognition of meteoric sphaerosiderite lines (MSLs) (Ludvigson et al. 1998). Sphaerosiderites are millimeter-scale $FeCO_3$ spherulites that formed in ancient wetland soil environments. MSL's are trends defined by sphaerosiderite isotopic compositions with invariant $\delta^{18}O$ values and highly variable $\delta^{13}C$ values (Ludvigson et al. 1998). The MSLs are analogous to the meteoric calcite lines of Lohmann (1988). The constant $\delta^{18}O$ values reflect precipitation in a well-developed groundwater system with stable oxygen isotope ratios and uniform temperature (Hays and Grossman 1991; Ludvigson et al. 1998).

Recently, $\delta^{18}O$ values of sphaerosiderite latitudinal gradients have been determined for the Albian of the Western Interior Basin (Ludvigson et al. 1998; White et al. in press). Reconstructing north–south latitudinal trends in Albian meteoric $\delta^{18}O$ compositions is one of the long-term goals of our research. The Albian meteoric $\delta^{18}O$ records we have compiled (including data presented in this paper) indicate that meteoric $\delta^{18}O$ values progressively decrease with increased paleolatitude (Ludvigson et al. 1998). Furthermore, the Albian $\delta^{18}O$ latitudinal gradient is steeper than that modeled for siderite forming in modern soil waters. It is widely accepted that much of the mid-Cretaceous was a time of global warmth or ''greenhouse'' conditions (Spicer and Corfield 1992; Francis and Frakes 1993; Glancy et al. 1993; Upchurch and Wolfe 1993). The steeper Albian meteoric $\delta^{18}O$ paleolatitudinal gradient is interpreted to have been a result of increased precipitation during this ''greenhouse'' period (Ludvigson et al. 1998), and it has been used to constrain estimates of the intensification of the mid-Cretaceous hydrologic cycle (White et al. in press). Ultimately, using MSLs from amalgamated sphaerosiderite-bearing paleosols like those presented here ($\delta^{18}O$ chemostratigraphic profiles), we hope to correlate isotopic trends throughout the Cretaceous Western Interior Basin (KWIB) and reconstruct precipitation $\delta^{18}O$ trends for shorter time intervals during the mid-Cretaceous.

Although there is a well-defined northward depletion in sphaerosiderite $\delta^{18}O$ values within any particular locality with multiple sphaerosiderite-bearing paleosols, there is systematic stratigraphic variability that reflects temporal changes during the Albian. The amalgamated sphaerosiderite-bearing paleosols of the Boulder Creek Formation are ideal for investigating this stratigraphic variation (Figs. 1, 2).

In this paper we explore some possible causes for temporal variability of sphaerosiderite $\delta^{18}O$ values in the amalgamated paleosols of the Boulder Creek Formation. Paleosol micromorphological characteristics and sphaerosiderite minor-element data facilitate evaluation of the temporal variations in sphaerosiderite $\delta^{18}O$ values. We hypothesize that the isotopic variability (positive $\delta^{18}O$ excursions) through some sphaerosiderite-bearing paleosols may be related to changes in alluvial base level.

Boulder Creek Formation

As shown by Leckie et al. (1989) the upper 90 meters of the Late Albian (Fig. 1) Boulder Creek Formation consists of nonmarine, alluvial mudstones and siltstones that were subjected to extensive pedogenic modification. The paleosols developed in floodplain deposits shed from the Cordillera to the southwest (Leckie et al. 1989; Leckie and Reinson 1993). There are 15 superposed paleosols and pedocomplexes in the nonmarine Boulder Creek Formation of the Monkman Pass area (Leckie and Foscolos 1986; Leckie et al. 1989; Stelck and Leckie 1988, 1990; Leckie and Reinson 1993). In general, the paleosols exhibit drab gray colors, root traces, pedogenic slickensides, blocky structure, clay coatings, mottling, and sphaerosiderite. The drab gray colors, manganese mottles, and abundance of sphaerosiderites suggest that many of these paleosols formed in poorly drained environments (Leckie et al. 1989; Leckie and Reinson 1993). Leckie and Reinson (1993) suggest that the waterlogged paleosols may have resulted from topographic position on a low-relief alluvial plain with broad, gently sloping divides.

Leckie et al. (1989) described the paleosols in detail, and paleosol complex 1 (67–74 m in Figure 3) is of particular importance to this investigation (Table 1 of Leckie et al. 1989). Several sphaerosiderite-bearing samples obtained for this study were acquired from paleosol complex 1, spe-

JOURNAL OF SEDIMENTARY RESEARCH, VOL. 71, NO. 6, NOVEMBER, 2001, P. 1017–1028
 1527-1404/01/071-1017/$03.00

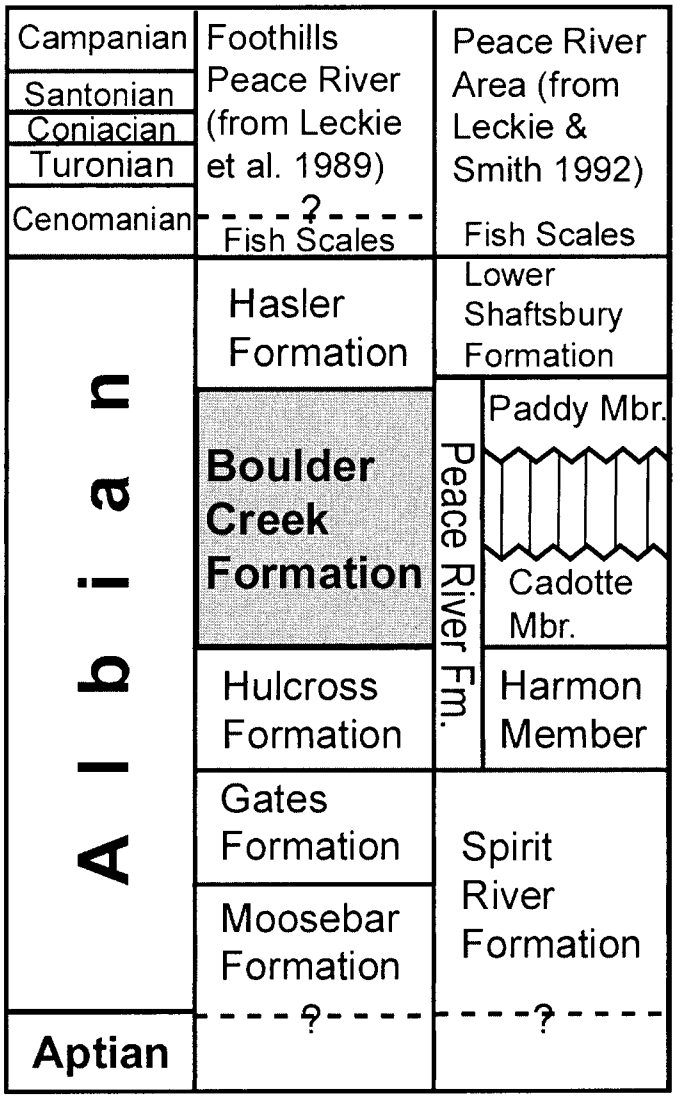

FIG. 1.—Stratigraphic correlation chart for the mid-Cretaceous in the Peace River area of Alberta and British Columbia (modified from Leckie and Smith 1992).

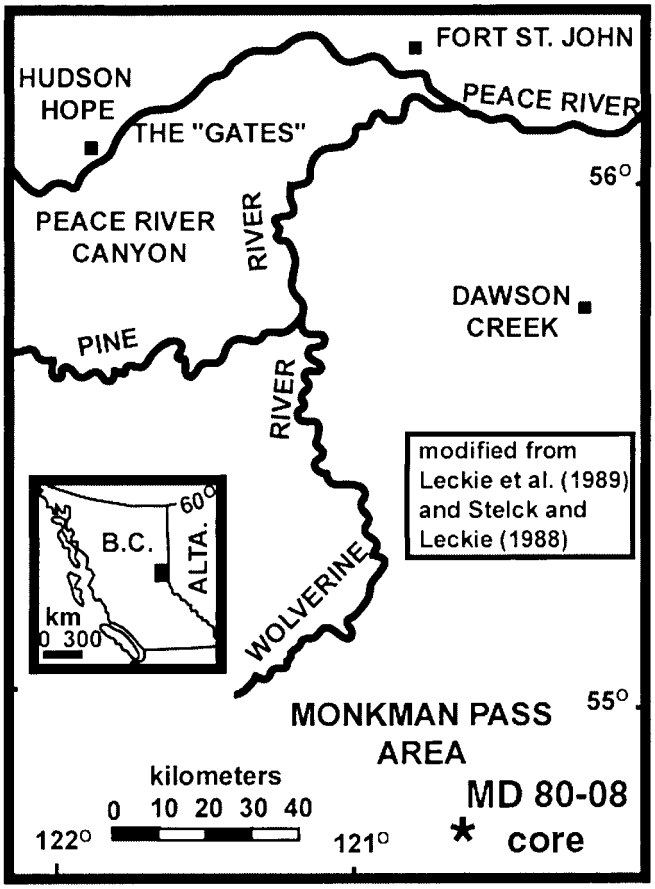

FIG. 2.—Location of the Boulder Creek Formation Monkman Pass (MD 80-08) core in British Columbia, Canada (modified from Stelck and Leckie 1988 and Leckie et al. 1989).

cifically from the 68.6–69.75 m depth interval (described in detail below) (Fig. 4). Leckie et al. (1989) subdivided paleosol complex 1 into 11 pedogenic horizons following the Canadian system of soil classification (Agriculture Canada Expert Committee on Soil Survey 1987), and the 68.6–69.75 m samples we collected are from their Bt3 and II Bm (equivalent to Bw of the U.S.D.A. classification scheme) horizons (Table 1 of Leckie et al. 1989). Figure 4 summarizes the macromorphological features we observed in paleosol complex 1.

METHODS

Lithologic descriptions and samples were collected from the Monkman Pass MD 80-08 coal exploration core curated at the Geological Survey of Canada core facility in Calgary, Alberta. A total of 30 sphaerosiderite-bearing paleosol horizons were sampled, and the position of each sample is marked with an asterisk adjacent to the lithologic log of Leckie et al. (1989) illustrated in Figure 3. At least 10 isotopic analyses of sphaerosiderites were conducted on each of the 30 sampled horizons. Micromorphological analyses were also performed on all 30 horizons (following the methods of Bullock et al. 1985), but sampling limitations prevented complete, detailed analysis of any particular paleosol complex. The fairly dense sampling between 68 and 70 m (Fig. 3) did permit detailed examination of part of paleosol complex 1 of Leckie et al. (1989) (described in detail below).

Confirmation of unaltered, early diagenetic sphaerosiderite was evaluated using light microscopy, cathodoluminescence petrography, epifluorescence petrography, and scanning electron microscopy. Polished slabs from each of the 30 paleosol horizons were microsampled using a microscope-mounted drill assembly with a 0.5 mm drill bit. All samples extracted for mass spectrometry were analyzed at the University of Iowa Paul H. Nelson Stable Isotope Laboratory.

Powdered samples were vacuum-roasted at 380°C to remove volatile contaminants. Samples were then reacted with anhydrous phosphoric acid at 72°C in an on-line automated Kiel III carbonate reaction device coupled to the inlet of a Finnigan MAT 252 isotope-ratio mass spectrometer. All isotopic values were reported relative to the PeeDee Belemnite (PDB) standard, with analytical precision of better than $\pm$ 0.05‰ for carbon and oxygen. Siderite data were corrected with the experimentally determined temperature-dependent isotope fractionation factor of Carothers et al. (1988).

Electron microprobe analyses were conducted on sphaerosiderites from 16 separate horizons using a JEOL JXA-8900R electron microprobe at the University of Minnesota. Siderite analyses were performed using wavelength-dispersive spectrometry at an accelerating voltage of 15 kV, a beam current of 10 nA, and with a beam diameter of 5 μm. The following X-

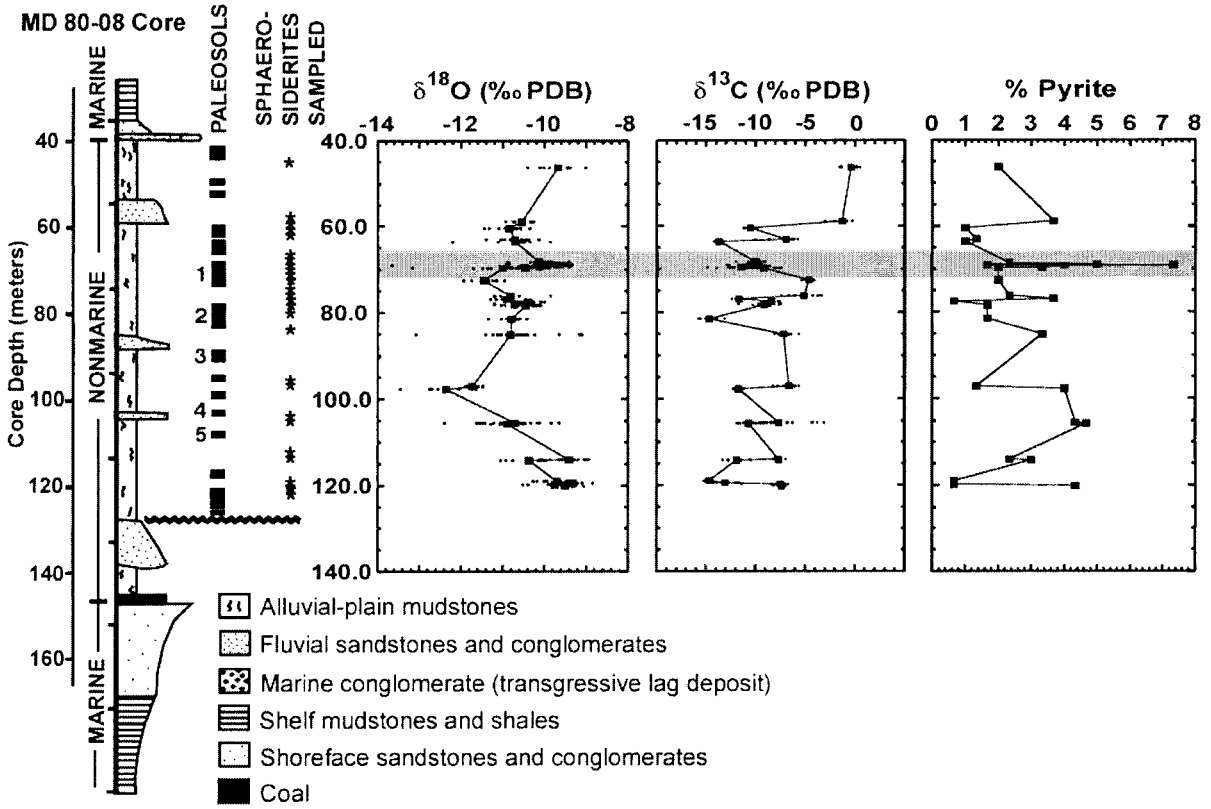

FIG. 3.—The lithostratigraphy, interpreted depositional environments, and paleosols of the Boulder Creek Formation Monkman Pass (MD 80-08) core (modified from Leckie et al. 1989). The paleosols noted by Leckie et al. (1989) are marked with black rectangles adjacent to the lithologic log, and paleosol complexes 1–5 are labeled. The asterisks represent the 30 sphaerosiderite-bearing samples collected for this study. The first two graphs illustrate oxygen and carbon isotope curves generated from analyses of meteoric sphaerosiderites. Each large square on the graphs is the average of 10 isotopic analyses (small filled circles) (error is < 0.1‰). PDB is the Pee Dee Belemnite standard. The third graph (on the far right) represents the percentage of sedimentary pyrite observed in 28 of the 30 sphaerosiderite-bearing horizons. Two units were not counted because of poor thin section quality, but visual estimates of polished slabs indicate a low percentage of pyrite ($< 3\%$). Point counts of 300 grains per slide were made following traditional point-counting methods. The shaded area denotes the 69.75–68.6 m depth interval.

ray lines and standards were used: $Ca_{K\alpha 1}$ (Calcite), $Mg_{K\alpha 1}$ (dolomite), $Mn_{K\alpha 1}$ (rhodonite), $Fe_{K\alpha 1}$ (siderite), and $Sr_{K\alpha 1}$ (strontianite).

RESULTS

Stable Isotopes of Oxygen and Carbon

Oxygen Isotopes.—The average $\delta^{18}O$ values for all of the sphaerosiderite-bearing horizons fall between -12.37 and -9.32 ‰ (PDB). Carbon and oxygen isotope plots for each horizon commonly show invariant trends in the $\delta^{18}O$ values. Standard deviations in the $\delta^{18}O$ values from individual horizons range from 0.15 to 0.62‰ with an average value of 0.35‰.

The sphaerosiderite data were compiled into a chemostratigraphic $\delta^{18}O$ profile of the alluvial section of the Boulder Creek Formation (Fig. 3). Some noteworthy trends in this curve especially the positive 1.31‰ excursion between the 69.75–68.6 m depth interval, are discussed below.

Carbon Isotopes.—The carbon isotope compositions of the sphaerosiderites are more variable than the oxygen isotope compositions. Average $\delta^{13}C$ values through the core range from -14.72‰ to -0.38‰ (PDB), with the most enriched values occurring at the top of the alluvial section (Fig. 3). Standard deviations in $\delta^{13}C$ values within a given horizon range from 0.20 to 2.11‰, with an average value of 0.80‰.

Carbon and oxygen isotope plots from individual horizons commonly show trends of both: (1) invariant $\delta^{18}O$ and $\delta^{13}C$ values, and (2) linear trends of invariant $\delta^{18}O$ and more variable $\delta^{13}C$ values (Fig. 5).

Meteoric-Water Compositions.—Using several of the least variable MSLs (those with $\delta^{18}O$ standard deviations < 0.3‰), and the range of likely paleotemperatures for this paleolatitude from Barron (1983), a range of groundwater $\delta^{18}O$ values have been estimated (Fig. 6). The groundwater $\delta^{18}O$ values were modeled using maximum and minimum paleotemperature estimates for the KWIB from 52° N latitude (approximate position of Monkman Pass area during the Late Albian) and the ^{18}O fractionation equation of Carothers et al. (1988). The $\delta^{18}O$ values of the Boulder Creek Formation groundwater ranged between -16‰ and -11‰ (SMOW).

Minor Elements

The sphaerosiderites analyzed were all greater than 80 mol % $FeCO_3$, with minor enrichments in Ca, Mg, Mn, and Sr (Fig. 7). Peaks in Mg substitution occur at the 69.75 m and 97.7 m depth intervals (2.92 and 7.15 mol % $MgCO_3$, respectively), and a peak in Ca also occurs at a depth of 97.7 m (15.40 mol % $CaCO_3$). Manganese substitution is generally less than 5 mol % $MnCO_3$, with the exception being at the 105.7–105.5 m interval, where up to 39.87 mol % $MnCO_3$ is present. The Sr concentrations were generally very low, with a peak substitution of 0.06 mol % $SrCO_3$ at the 97.7 m horizon. Comparison of Mg/(Ca + Mg) and Mg/Fe ratios show relative compositional trends through the alluvial section (Fig. 8).

Paleosol Micromorphology

Paleosol micromorphology is an invaluable tool for extracting paleoclimatic information (e.g., Ashley and Driese 2000; Caudill et al. 1996; Driese and Foreman 1992; Elick et al. 1998; Mora et al. 1991; Retallack and Mindszenty 1994), understanding alluvial architecture and floodplain dy-

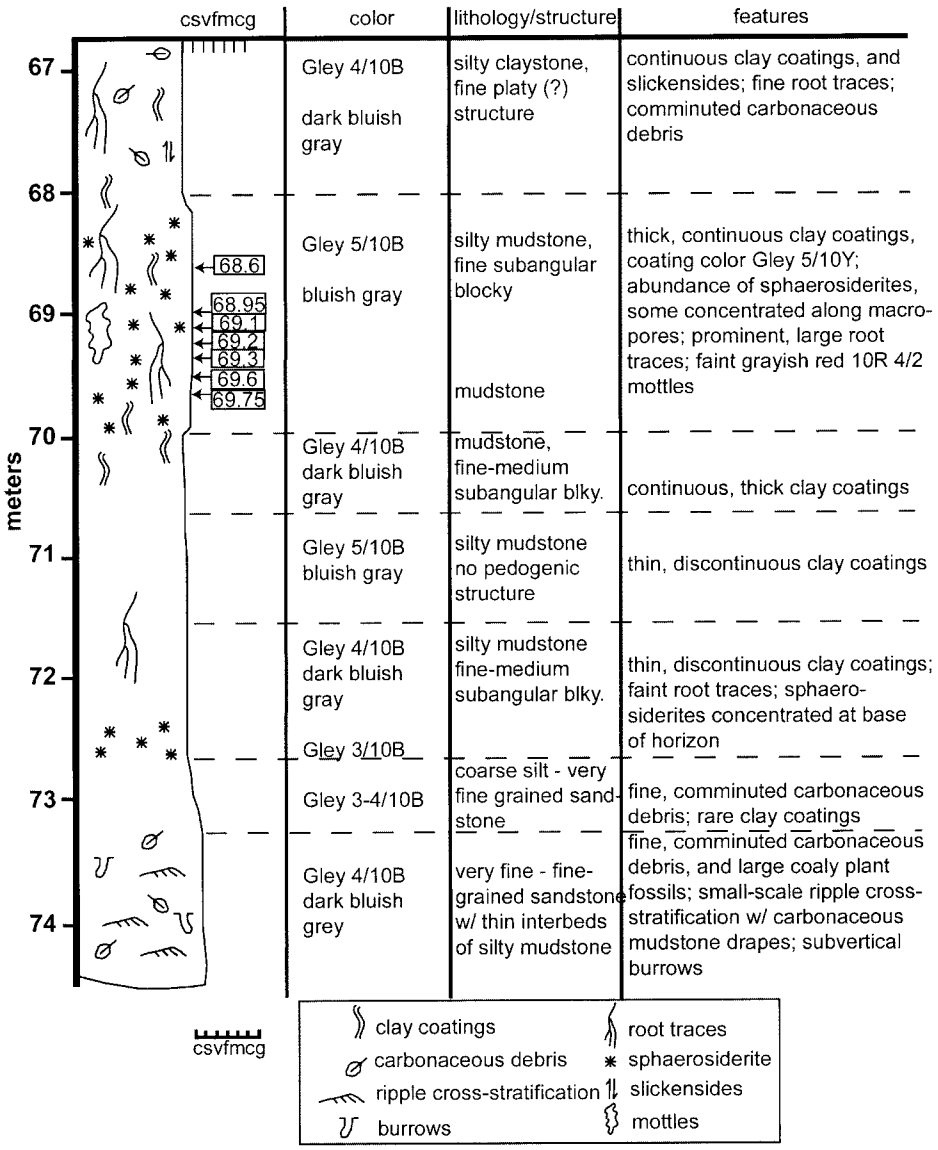

FIG. 4.—Lithologic and pedogenic description of the 67–74 m depth interval (paleosol complex 1 of Leckie et al. 1989) of the MD 80-08 core. Refer to Figure 3 for the stratigraphic position of this depth interval in the alluvial section of the Boulder Creek Formation. The position of the samples used to complete the detailed micromorphological analysis described in the text are labeled directly adjacent to the graphic log (boxes with arrows).

namics, and recognizing sequence boundaries (Bestland 1997; Bestland et al. 1997; Driese et al. 1992; Kraus and Aslan 1993; Kraus 1997, 1999; McCarthy and Plint 1998; McCarthy et al. 1997a, 1997b; McCarthy et al. 1998a, 1998b; McCarthy et al. 1999a, 1999b; Wright 1994).

Micromorphological characteristics were described for each of the 30 sphaerosiderite-bearing units and, aside from the fact that they all contain sphaerosiderite, some features were common to all of the examined paleosols. In general, all of the units are clay-rich mudstones with quartzose, silt-size framework grains in varying modal abundances, and characterized by cross-striated birefringence fabrics (sepic plasmic fabrics of Brewer 1964). Compound, dense, complete clay and silty-clay infillings and typic clay coatings (argillans of Brewer 1964) with sesquioxide hypocoatings (neo-cutans of Brewer 1964) are common. Often the clay coatings and infillings exhibit evidence of degradation and reworking. Small, cube-shaped, silt-size pyrite nodules are ubiquitous, and are found as inclusions in sphaerosiderites, disseminated throughout the matrix, or (less commonly) as pseudomorphs after organic matter. The sphaerosiderites generally occur as either: (1) individuals; (2) linear arrays of nodules; (3) pseudomorphs of root traces, or disseminated organic fragments; or (4) tight clusters where the boundaries of individuals have become diffuse.

The oxygen isotope excursion (Fig. 3) generated from the seven closely spaced, sphaerosiderite-bearing paleosol samples in the 69.75–68.6 m depth interval (paleosol complex 1 of Leckie et al. 1989) (Figs. 3, 4) prompted a more detailed micromorphological analysis. A brief description of the micromorphological characteristics observed in the 69.75–68.6 m depth interval is given below.

Root Traces.—Vertical to subvertical, bifurcating, carbonaceous root traces are observed throughout the paleosol at the macroscale (Fig. 9). In thin section, numerous, thin (generally less than 10 μm), carbonaceous root traces are observed, often in association with clay coatings. Commonly, the fine root traces are discontinuous and randomly oriented. At 69.75 m, numerous organic fragments are present; these may represent comminuted organic matter or oblique slices through prominent root traces.

Mineral Components.—The coarser-grained material generally consists of moderately well sorted, subangular to subrounded, quartzose ($>$ 90%) siltstone to very fine-grained sandstone. Minor amounts of muscovite, biotite, chert, altered feldspar grains, lithic rock fragments, ferruginous oxides, and sulfides are also present. The finer-grained material consists of a variety of clay minerals, including kaolinite and mixed-layer clays (Leckie et al. 1989).

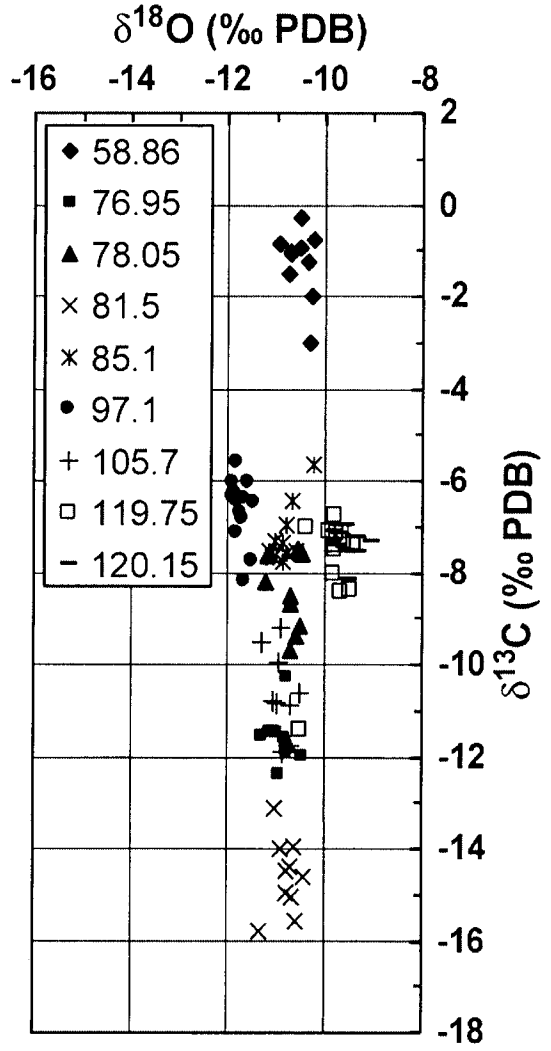

FIG. 5.—Stable-isotope compositions of sphaerosiderites from several depth horizons in the alluvial section of the Boulder Creek Formation. Each unit defines trends of relatively invariant $\delta^{18}O$ values and more highly variable $\delta^{13}C$ values or low variance in both $\delta^{18}O$ and $\delta^{13}C$ values (meteoric sphaerosiderite lines; MSLs).

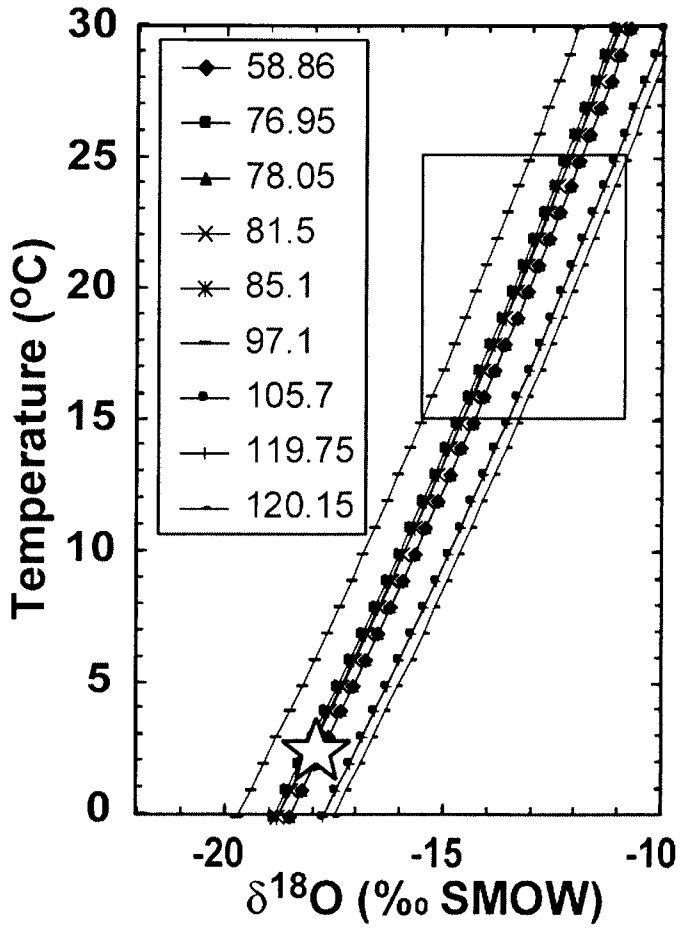

FIG. 6.—Soil groundwater $\delta^{18}O$ values calculated from Boulder Creek Formation meteoric sphaerosiderite lines. The rectangle defines the range of maximum and minimum mean annual temperatures for the mid-Cretaceous at 52° N latitude determined using a 4 × CO_2 atmosphere paleoclimate model simulation (acquired from Barron 1983). The star represents the present mean annual temperatures at 52° N latitude. SMOW is standard mean ocean water.

Groundmass.—Two primary textural domains are recognized. To simplify descriptions, the finer-grained component will be referred to as claystone and the coarser-grained component as siltstone.

Claystone Domains.—The claystone is slightly silty (generally fine silt) and exhibits speckled and cross-striated birefringence fabrics (*b* fabrics) (Fig. 10A). Generally, the elongate zones of oriented clay that define striations exhibit at least two preferred orientations that cross at high angles. The striations are thin (10–20 μm thick) and discontinuous. Some speckled *b* fabrics are present where very small ($<$ 10 μm thick) elongated zones of oriented clay are observed randomly distributed throughout the claystone domains. Similar claystone fabrics are observed throughout the alluvial section.

Siltstone Domains.—The siltstone component is generally a framework-supported, moderately well sorted, subangular to subrounded, quartzose siltstone to very fine-grained sandstone with a very fine silty-clay interstitial matrix (Fig. 10D, E).

Intercalations between the siltstone and claystone fabrics characterize the 69.75–68.6 m depth interval (Fig. 10D, E). The lowest unit (69.75 and 69.6 m) is characterized by claystone. Between 69.4 and 68.95 m, the siltstone and claystone are intercalated on a centimeter scale with sharp boundaries between the groundmass fabrics. In places the siltstone completely (or nearly so) surrounds clasts of the claystone (Fig. 10E). The enveloped claystone domains (millimeter scale) have rounded to prolate shapes. In the uppermost unit (68.6 m) the overall fabric is a complex mosaic of the siltstone and claystone domains (millimeter scale) with diffuse boundaries.

Intercalated matrix fabrics of siltstone and claystone domains were also observed in the 114.2 m, 119.0 m, and 119.45 m depth intervals.

Coatings.—Void coatings of clay, organic matter, and sesquioxides are common in all of the sampled paleosols in the MD 80–08 core. In the 69.75–68.6 m depth interval, void coatings are generally confined to the claystone domains.

Typic (coatings that are approximately equal in thickness throughout their length) clay coatings are generally thin (10–30 μm in thickness), and discontinuous throughout the claystone domains (Fig. 10A, B). The coatings exhibit diffuse extinction patterns, and are composed of moderately oriented, first-order birefringent clays. The clay coatings generally have gradational boundaries with the adjacent matrix, and are commonly fragmented and incorporated into the matrix (Fig. 10A, B).

Juxtaposed on many of the typic clay coatings are very thin, typic, opaque, organic coatings (organans of Brewer 1964). The organic coatings are discontinuous, and do not exceed a few microns in thickness. Commonly associated with the typic organic coatings are diffuse, black to

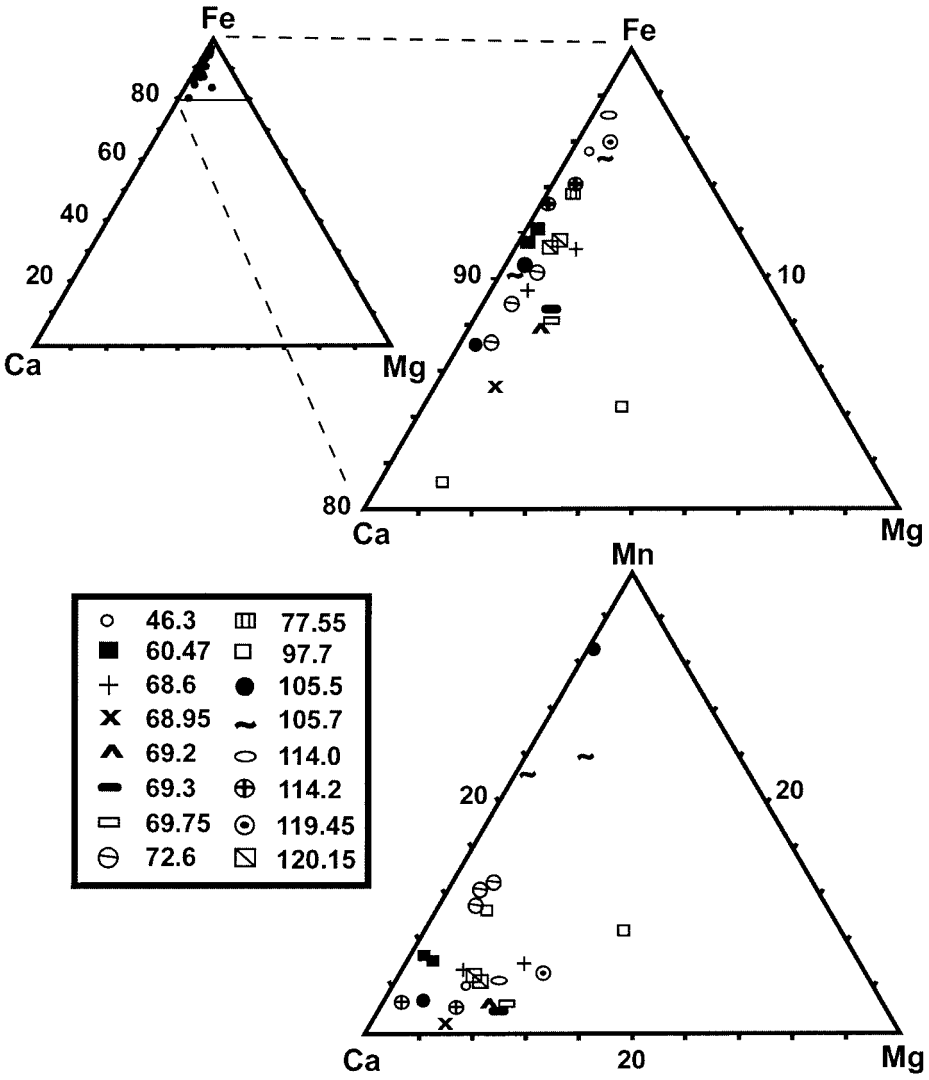

FIG. 7.—Ternary diagrams comparing $FeCO_3$–$MgCO_3$–$CaCO_3$, and $CaCO_3$–$MnCO_3$–$MgCO_3$. All of the samples analyzed were > 80 mol % $FeCO_3$.

smoky-gray, manganese oxide hypocoatings that weakly impregnate the typic clay coatings or adjacent matrix. Less commonly observed are weakly impregnative, superimposed, sesquioxide (orange-brown) hypocoatings. Some rare, loose, incomplete pyrite void coatings were also observed.

Infillings.—Infillings are less common than coatings, and generally consist of dense, complete, clay and silty-clay laminae that fill millimeter-scale channels (Fig. 10C). Commonly, the channels have conical to crescentic shapes and sharp boundaries with the adjacent matrix. Laminae are composed of moderately oriented, second-order birefringent clays, and silty clays. Juxtaposed on some of the laminae are very thin, opaque, carbonaceous coatings and some dark brown ferruginous hypocoatings. Commonly, the laminae and/or the whole channel appear to be deformed. In a few cases (e.g., 68.6 m), the infillings are highly deformed, fragmented, and incorporated into the matrix.

Nodules.—Pyrite abundance is greatest between 69.3 and 68.95 m (maximum of 8% based on 300-point-count survey) (Fig. 3), and occurs as small (10–30 μm), cubic to subrounded, crystalline forms disseminated throughout the groundmass (Fig. 10F). Pyrite occurs in both the claystone and siltstone domains, although its abundance is greatest in the former. It is opaque and isotropic, and has high relief under transmitted light, and shows characteristic brassy metallic luster in reflected light. The pyrite most often occurs as disseminated individual cubic forms (20–30 μm), clusters or arrays of cubic to subrounded forms, and inclusions within sphaerosiderites (discussed further below).

Sphaerosiderite is abundant and generally has a typic, crystalline (some geodic), radial concentric microstructure. Sphaerosiderites range from approximately 200 to 1250 μm in size, and occur as individuals, clusters, and arrays of nodules (Fig. 10E, F, Fig. 11A–D). The nodules are typically microcrystalline on the interior, and fibrous on the exterior. Many nodules exhibit opaque to dark brown-orange, ferruginous rings (quasi-coatings) within the nodule (Fig. 11D), some of which contain 10–20 μm pyrite nodules. Pyrite cubes and dendritic forms are commonly observed in the cores and cortices of sphaerosiderites. Sphaerosiderites formed within both the claystone and siltstone domains, and on void coatings and infillings. The nodules crosscut sharp textural boundaries within the groundmass. In the 69.75 m unit, sphaerosiderite growth engulfed fossil plant material, preserving some of the cellular structure (Fig. 11A–C).

The 69.75 m unit contains an abundance of the 200–1250 μm nodules that fit the above descriptions, and a second much smaller, earlier generation of sphaerosiderite. The small nodules are 10–30 μm in size and occur as individual spherulites disseminated throughout the matrix and as linear arrays. The characteristic pseudo-uniaxial cross extinction pattern can be seen under high magnification in cross-polarized light. Linear arrays of the smaller spherulites are engulfed by some of the larger sphaerosiderites. The

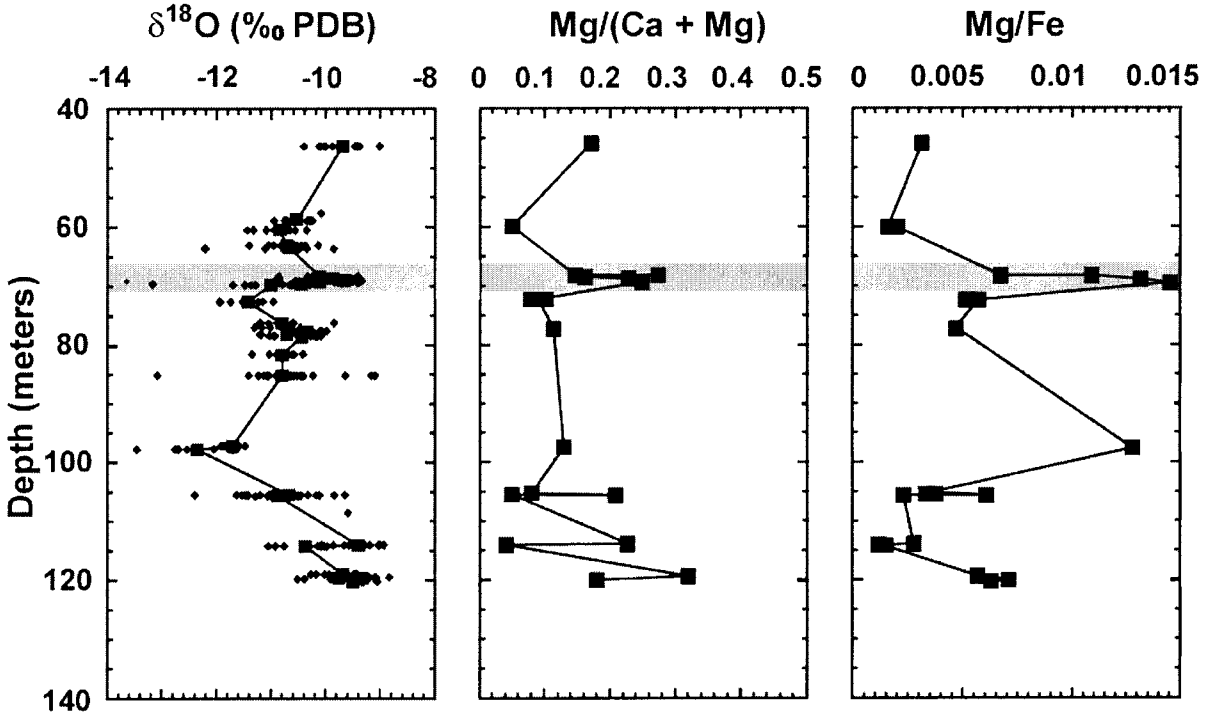

FIG. 8.—Graphs illustrating the stratigraphic distribution of Mg, Ca, and Fe cation ratios in the 16 analyzed sphaerosiderite-bearing horizons. Note the correlation between the positive $\delta^{18}O$ excursion between 68 and 70 m and the peaks in Mg/(Ca + Mg) and Mg/Fe ratios (shaded rectangle).

smaller nodules also nucleated on fossil plant material (roots) and are typically succeeded by overgrowths of larger sphaerosiderites (Fig. 11A–C).

DISCUSSION

Oxygen Isotopes

The $\delta^{18}O$ values for all of the MD 80-08 sphaerosiderites (average for all horizons = −10.4‰ PDB) suggest formation in meteoric phreatic groundwaters recharged by local precipitation. Significantly more depleted compositions would be expected if the soil water had been recharged by regional runoff from alpine meltwaters in the adjacent Cordillera (Dettman and Lohmann 2000; Glancy et al. 1993; Bloch 1990; Carpenter et al. 1988). Furthermore, the pervasive gleyed character of the paleosols suggests that evaporative enrichment of ^{18}O in the soil groundwater was negligible.

The chemostratigraphic excursions toward heavier $\delta^{18}O$ values may be a consequence of marine and meteoric water mixing. If marine $\delta^{18}O$ values were approximately −1 to −1.2‰ (SMOW) (Shackleton and Kennett 1975), infiltration and mixing of marine water with the soil (meteoric) water should increase $\delta^{18}O$ values in proportion to the degree of mixing. Subsequently, siderite precipitated from mixed fluids would have heavier $\delta^{18}O$ values.

Within individual sphaerosiderite-bearing units, mixing of two or more diagenetic fluids should have resulted in hyperbolic trends of $\delta^{18}O$ and $\delta^{13}C$ values varying between meteoric and marine end-member compositions (e.g., Carpenter et al. 1988; Lohmann 1988). The isotopic compositions of sphaerosiderites from the 69.75–68.6 m interval generally do not exhibit hyperbolic compositional trends, with one exception at 68.6 m. This unit has two distinct clusters of data that can be fitted to a hyperbolic mixing curve (Fig. 12). As discussed below, this unit also records a high Mg/(Ca + Mg) ratio. The enriched $\delta^{18}O$ cluster represents sphaerosiderites precipitated from meteoric compositions modified by marine fluid mixing, and the depleted $\delta^{18}O$ cluster is interpreted to represent pure meteoric compositions (Fig. 12). Our calculations show that the percentage of seawater mixing was less than 20%.

The remaining units in the 69.75–68.6 m interval have somewhat poorly defined MSLs with $\delta^{18}O$ standard deviations ranging from 0.2 to 0.55‰. Although hyperbolic fluid mixing trends are not evident in these units, the lightest end-member compositions probably represent pure meteoric compositions and the heavier values represent marine-modified meteoric compositions.

The sphaerosiderite isotopic compositions alone do not justify precipitation from marine-modified meteoric fluids. Many other factors, such as changes in temperature, regional water balance (evaporation and precipitation fluxes), source water isotopic compositions, and precipitation amount effects could account for the temporal variability in the $\delta^{18}O$ compositions (Dansgaard 1964; Gat and Matsui 1991; Rozanski et al. 1993). These factors may have contributed to the trends in $\delta^{18}O$ values, but the paleosol micromorphology and sphaerosiderite minor-element chemistries discussed below strongly suggest that marine fluids affected the siderite $\delta^{18}O$ compositions.

Paleosol Micromorphology (69.75–68.6 m)

Paleosol micromorphology was used to further interpret the oxygen isotope excursion between the 69.75 and 68.6 m depth interval that records an enrichment of approximately 1.31‰ (Fig. 3). The micromorphological features in this interval contain an archive of pedogenic changes forced by changes in base level.

The presence of compound clay coatings in the claystone fabric suggests that illuviation was a significant pedogenic process in this interval. The microlaminated coatings developed by eluviation from overlying soil horizons and progressive translocation and deposition of clay-size particles in lower horizons (FitzPatrick 1984; McCarthy and Plint 1998; McCarthy et al. 1998b). The presence and abundance of clay coatings indicates that the soil was well drained for some time (McCarthy et al. 1999b). Fragmenta-

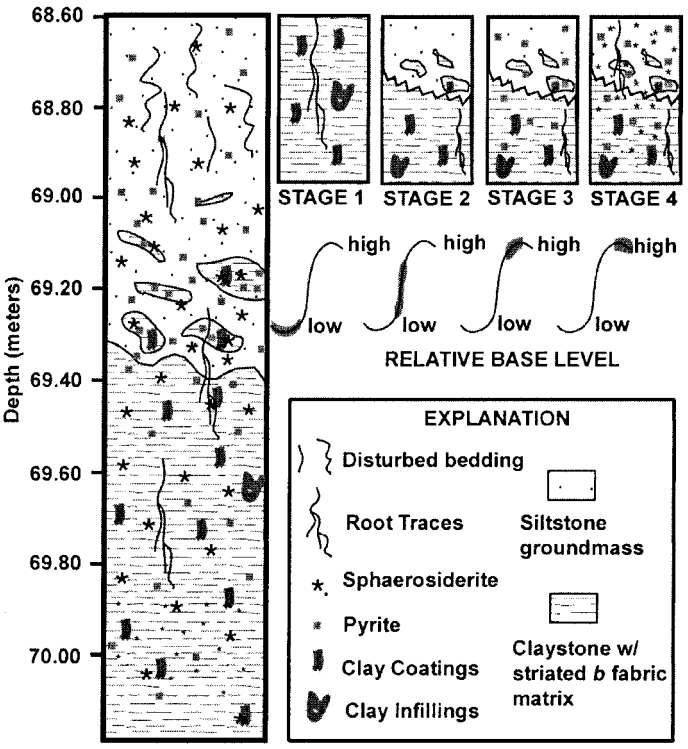

FIG. 9.—Cartoon illustrating the generalized pedogenic features and fabrics observed in the 69.75–68.6 meter depth interval of the MD 80-08 core. The stages represent the polygenetic pedogenic history and corresponding relative baselevel changes associated with development of this portion of the paleosol complex. In general, pedogenesis was influenced by: (Stage 1) a stable phase characterized by episodic wetting and drying, fluctuating water table, and relatively low baselevel; (Stage 2) a rise of baselevel, erosion of soil material, and deposition of coarser sediment; (Stage 3) high baselevel, saturated (reducing redox) conditions, and mixing of marine and meteoric fluids, pyrite precipitation; (Stage 4) high baselevel, saturated soils, reducing redox conditions, sphaerosiderite precipitation.

tion, discontinuous grainy extinction patterns, and assimilation of coatings into the surrounding matrix suggests prolonged landscape stability. These features reflect extensive shrink–swell reorganization of the soil and bioturbation (FitzPatrick 1984; McCarthy et al. 1998b; McCarthy et al. 1999a). Leckie et al. (1989) also noted extensive reorganization of the paleosol materials and translocation of clays. The striated *b* fabric prevalent in the claystone further substantiates shrink–swell reorganization of the soil during wetting–drying cycles (McCarthy and Plint 1998). The ferruginous hypocoatings may also reflect wet–dry cycles, and they further suggest some fluctuations in redox conditions (McCarthy et al. 1998b). The very thin, opaque carbonaceous coatings are fossil root fibers. Degraded argillaceous coatings and infillings are not unique to the 69.75–68.6 m depth interval; they are found in nearly all of the sampled paleosols of the MD 80-08 core.

The distinct textural change (also identified by Leckie et al. 1989) (Fig. 10D) and siltstone–claystone intercalations noted in the 69.3–69.4 m unit may reflect an episode(s) of erosion and flood deposition on the alluvial plain (McCarthy and Plint 1998). The rounded domains of claystone enveloped in siltstone are intraclasts ripped up directly from the subjacent clay-rich paleosol horizon. The claystone clasts were unlithified, cohesive units as shown by the overprinting of pyrite and sphaerosiderite nodules. The intercalated siltstone and claystone units have sharp boundaries in the lower parts of the pedocomplex, but they become increasingly more homogenized upsection. Fabric trends suggest that deposition of the siltstone was preceded by periods of floodplain erosion. Claystone intraclasts were eroded from the underlying material, yet sustained little transport and reworking. The paleosol was at least 80 cm thick, and postdepositional mixing seems to have been most prevalent in the upper 40 cm of the soil, where textural domains were homogenized by bioturbation and/or shrink–swell processes (68.6 m).

The ubiquitous, well-developed sphaerosiderites indicate that the pedocomplex was at times a poorly drained, hydromorphic soil (McCarthy and Plint 1999). Sphaerosiderites crosscut matrix fabrics as well as coatings and infillings, thus they formed later. The very small (10–30 μm) spherulites observed in the 69.75 m unit, however, are an exception. These nodules were overprinted by the larger spherulites, and they represent an earlier stage of hydromorphism.

The internal oxidation rings within some sphaerosiderites suggest periods of improved drainage due to water table fluctuations, or perhaps influxes of oxygenated fluid (McCarthy and Plint 1998). The presence of oxidation rings (quasicoatings) in some sphaerosiderites but not others implies relative age differences between nodules. The oxidation rings may represent brief hiatuses in siderite precipitation, or multiple stages of development as suggested by Leckie et al. (1989). The presence of very small (< 10 μm) pyrite inclusions lining some ferruginous quasi-coatings suggests that sulfate-rich waters (marine) episodically infiltrated the soils (Wright 1986).

The pyrite present in the pedocomplex may have been derived from weathered parent material, but it is much more likely that it formed *in situ* (FitzPatrick 1984). Pyrite is observed within many siderite nodules, suggesting that the sphaerosiderites formed later, engulfing matrix pyrite as they precipitated.

Precipitation of siderite and pyrite may have oscillated with the production of H_2S by sulfate-reducing bacteria in the soil water. There was an abundance of both iron and organic matter available in the system, thus sulfate availability was likely the limiting factor on the formation of pyrite over siderite (Carpenter et al. 1988). Alternatively, siderite may have followed pyrite after all available sulfate was reduced, leading to methanogenesis (Berner 1981; Pye et al. 1990). If methane oxidation had been an important process, the $\delta^{13}C$ values in this interval should be very depleted (-20 to -60‰ PDB). The values obtained, however, are well within the range of organic-matter degradation (Fig. 3) (Pye et al. 1990). The presence and abundance of pyrite suggests that marine fluids episodically infiltrated the paleosols (Wright 1986), and this process occurred with enough frequency and duration to result in extensive pyrite precipitation.

Pedocomplex History.—Micromorphological analysis of the sphaerosiderite-bearing units in pedocomplex I of Leckie et al. (1989) suggests a four-stage polygenetic development (Fig. 9).

Stage 1. Initially, the alluvial plain was characterized by a stable landscape with a fluctuating water table. This is shown by the well developed yet heavily degraded clay coatings present in the claystone matrix. The soil went through wet–dry cycles that disturbed and reworked coatings and infillings into the matrix. The striated *b* fabrics, and prominent illuvial clay coatings and infillings agree well with the Bt & Bm (Bw) soil horizon designations of Leckie et al. (1989). Baselevel during this stage in the soil development is interpreted to have been relatively low, prompting improved drainage of the soil during drier cycles. Occasional flooding of nearby fluvial channels may have provided a source of suspended-load clay particles, which subsequently were translocated through the soil profile.

Stage 2. An abrupt upward change in matrix fabric and the presence of claystone rip-up clasts at this boundary suggests erosion and subsequent deposition of coarser-grained material on the floodplain. Anastomosing systems are characterized by inhibited migration of fluvial channels, and a predominance of overbank deposits (e.g., levees, wetlands, and crevasse splays) (Smith and Smith 1980). Crevassing may lead to the development of new channels, and maintains dynamic anastomosing fluvial systems under conditions of rapid aggradation, and rising baselevel (Smith and Smith 1980). Perhaps crevassing provided the mechanism for removing some of

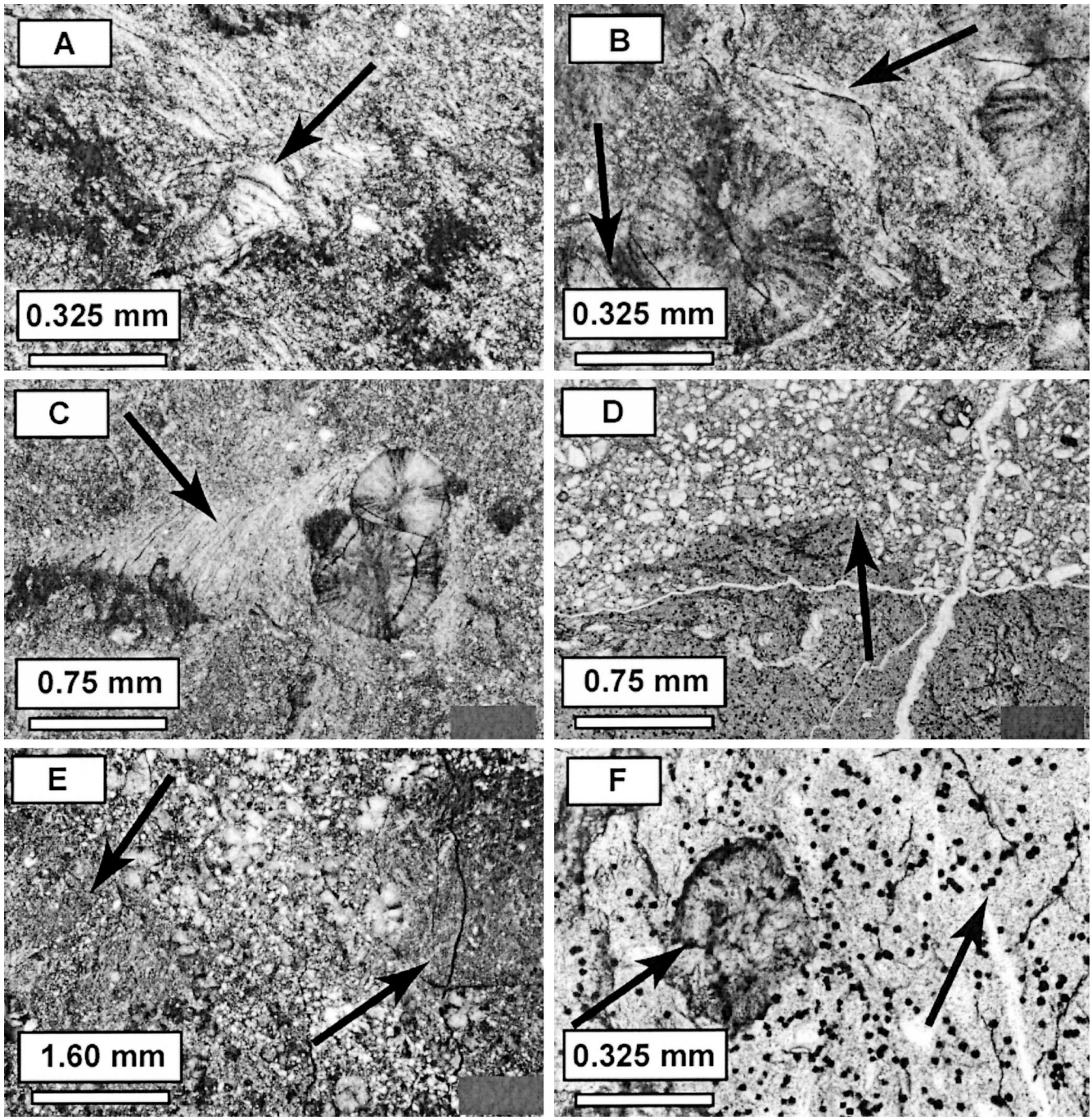

FIG. 10.—Photomicrographs exhibiting micromorphologic characteristics of paleosol complex 1 between 69.75 and 68.6 meters depth. **A)** Striated *b* fabric with thick, fragmented discontinuous clay coatings (arrow) under cross-polarized light (CPL). The clay coatings are disrupted and degraded, and were reworked into the surrounding matrix material perhaps via shrink–swell processes. **B)** Fragmented thick clay coatings (top arrow) in a striated *b* fabric groundmass with superimposed sphaerosiderites. Note the parallel, oxide-stained fractures between the sutured sphaerosiderites in lower left of the photo (arrow). **C)** Laminated clay infilling (arrow) with superimposed sphaerosiderites contained within a striated *b* fabric groundmass. **D)** Sharp boundary (arrow) separating the siltstone (upper half of photo with white quartz grains) and claystone (darker gray) matrix fabrics. The very small black grains are pyrite, and they are observed in both fabrics (more abundant in claystone). **E)** Sharp boundary between claystone and siltstone matrix fabrics under cross-polarized light. The siltstone fabric is dominated by the (white) quartz grains and abundance of sphaerosiderites (note the sphaerosiderites reside in both fabrics). The claystone clasts are rounded (designated by arrows), and the one on the right is nearly surrounded by the siltstone. **F)** Pyrite (arrow) observed in the claystone groundmass and in the cortex of a sphaerosiderite nodule (left arrow).

the topsoil and depositing coarser silts in the wetland soils as base level was rising.

Stage 3. The pyrite formed when marine water mixed with the soil pore fluids. During this stage, we suggest that a minor rise in sea level increased local baselevel and that the water table remained high enough to maintain saturated soil conditions. Perhaps marine–meteoric fluid mixing occurred through tidal pumping or storm surges (Ludvigson et al. 1996). The lack of preserved tidal sedimentary structures and marine fossils in the alluvial

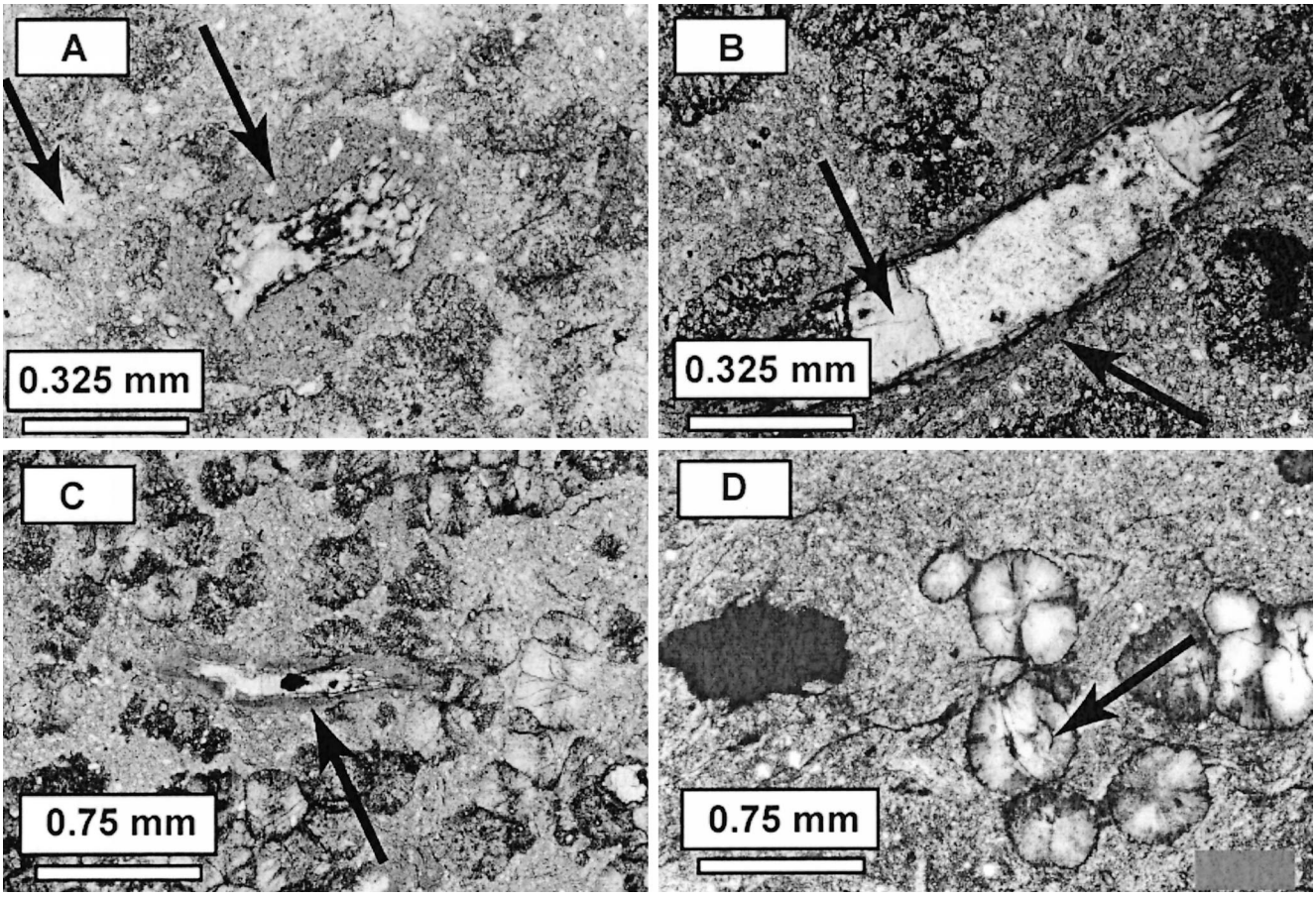

FIG. 11.—**A)** In the center of the photomicrograph is a fossil plant fragment (root) pseudomorphed by the very small sphaerosiderites (center arrow). Some of the plant cell structure has been preserved. Surrounding the fossil are several inclusion-rich larger sphaerosiderites (left arrow). **B)** Another example of siderite-pseudomorphed plant fragment (lower arrow) with internal dissolution and replacement by blocky siderite (upper arrow). The whitish area is filled with clay (possibly kaolinite). **C)** Low-magnification example of siderite-pseudomorphed plant material (arrow) showing relationship with the surrounding matrix. **D)** An array of sphaerosiderites superimposed on degraded, clay coatings in a striated *b* fabric claystone. Note the internal oxidation rings (quasi-coatings) in the sphaerosiderites in center of photomicrograph (arrow).

section of the Boulder Creek Formation (Stelck and Leckie 1990) suggests a transition to coastal wetland paleosols within a fluvial–estuarine setting, upstream from the open marine environment.

Stage 4. The final stage is marked by development of the sphaerosiderites. Baselevel remained high during sphaerosiderite formation, but the pore fluid was dominated by fresh water. The $\delta^{18}O$ values and minor-element compositions (discussed below) suggest that some minor mixing of marine and soil groundwater still occurred. The material overlying this interval consists of approximately four meters of gleyed mudstone with an abundance of carbonaceous material, prominent clay coatings, slickensides, and mottles. These features suggest very slow accumulation of sediment on the alluvial plain, perhaps through slow progradation of the system (resulting in a relative baselevel fall) and the return to a relatively stable landscape with cyclic wetting and drying phases.

The pedogenic history described above is not unique to the 69.75–68.6 m depth interval. Similar pedogenic histories coupled with $\delta^{18}O$ excursions can be interpreted in the 120.15–119.0 and 114.2–114.0 intervals (Fig. 3), but limited sampling precluded detailed micromorphologic analyses of those intervals.

Minor Elements

Sphaerosiderite cation concentrations from several horizons in the alluvial section of the Boulder Creek provide further insight into pedogenic processes. In the 69.75–68.6 m interval, there is excellent correlation between the peak (heavier) $\delta^{18}O$ values (−9.696‰), peaks in Mg/(Ca + Mg) and Mg/Fe ratios as well as the peak in modal percentage of pyrite (Fig. 8). Similarly, at 114.0 and 119.45 meters, there are increased Mg/(Ca + Mg) and Mg/Fe ratios that correspond with heavier (−9.411‰ and −9.322‰ respectively) $\delta^{18}O$ values.

The increased Mg and Ca concentrations in the sphaerosiderites of the 69.75–68.6 m interval provide additional evidence for mixing of marine and meteoric waters. Siderite precipitated in freshwater environments is typically very pure, containing greater than 90 mol % $FeCO_3$ (Mozley 1989). This is generally true for the Boulder Creek sphaerosiderite horizons with low Mg/Fe and Mg/(Ca + Mg) ratios (Fig. 8). Marine waters have higher Mg^{2+} and Ca^{2+} concentrations and greater Mg^{2+}/Ca^{2+} ratios than meteoric waters (Carpenter et al. 1988; Mozley 1989). Matsumoto and Iijima (1981) suggested that increased Mg/(Ca + Mg) ratios in siderite concretions from Paleogene coal measures of Japan resulted from precipitation in freshwater that mixed with Mg-rich brines from interbedded marine deposits.

At 97.7 m, peaks in Ca and Mg concentrations correlate with the most depleted $\delta^{18}O$ values in the section (Fig. 8). Diagenetic trends in ^{18}O and ^{13}C compositions suggest that the increased Mg, Ca, and Sr concentrations in this unit resulted from later diagenetic alteration of the sphaerosiderites, and not from early marine–meteoric fluid mixing.

Not all of the sphaerosiderite-bearing paleosols represent sea-level-driven changes in baselevel. Some of these units undoubtedly formed through

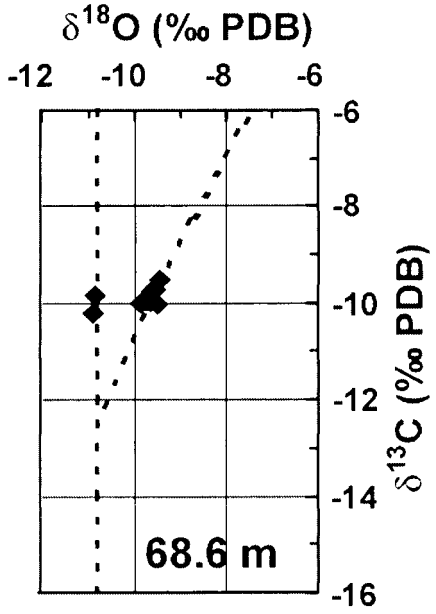

FIG. 12.—Equal-area plot of $\delta^{18}O$ vs. $\delta^{13}C$ for the 68.6 m horizon, illustrating two clusters of isotopic data, which define an MSL (straight vertical dashed line), and a marine-modified hyperbolic mixing trend (curved dashed line).

autocyclic changes within the alluvial system. The paleosols showing positive $\delta^{18}O$ excursions, micromorphologic characteristics indicative of base-level changes, an abundance of pyrite, and increased Mg/Fe and Mg/(Ca + Mg) ratios, however, strongly suggest marine influence on pedogenesis.

CONCLUSIONS

(1) Boulder Creek Formation sphaerosiderites are an early diagenetic product with $\delta^{18}O$ and $\delta^{13}C$ values that record formation in meteoric phreatic fluids recharged by local precipitation. The Boulder Creek Formation MSLs provide constraints for the isotopic composition of Late Albian shallow groundwaters of the western coastal plain of the KWIB, and yield $\delta^{18}O$ values that range from −11‰ to −16‰ SMOW. The sphaerosiderites provide a proxy record of Late Albian precipitation and can be used to quantify changes in the hydrologic cycle that result in depleted isotopic compositions of precipitation during humid Greenhouse periods (e.g., White et al. 2001).

(2) The +1.3‰ excursion in the sphaerosiderite $\delta^{18}O$ values through the 69.75–68.6 m interval resulted from minor marine–meteoric fluid mixing due to a rise in relative sea level. The abundance and close association of pyrite with the sphaerosiderite also suggests marine influence on pedogenesis. The MSLs through this interval have relatively large standard deviations (up to 0.55‰), and in one case (68.6 m) a hyperbolic fluid mixing trend is proposed. The depleted end-member $\delta^{18}O$ values from MSLs represent pure meteoric compositions, and the enriched represent marine-modified meteoric compositions. The extent of marine–meteoric fluid mixing was very low (< 20% marine water).

(3) Increased siderite Mg/(Ca + Mg) and Mg/Fe ratios relative to end-member (> 90 mol % $FeCO_3$) sphaerosiderite compositions provide additional evidence for marine–meteoric fluid mixing. Sphaerosiderites with the highest Mg compositions correspond to the heaviest $\delta^{18}O$ values, and peaks in modal abundance of sedimentary pyrite. This correlation is best noted in the 69.75–68.6 m interval, but it is also evident in the 120.15–119.0 and 114.2–114.0 m intervals.

(4) The alluvial part of the Boulder Creek Formation is aggradational, and it may represent the nonmarine component of a transgressive systems tract. The overall rise in relative sea level was punctuated by minor sea-level oscillations recorded in the micromorphology and siderite geochemistry of the paleosols.

ACKNOWLEDGMENTS

We are grateful to the Geological Society of America for a student research grant award made to the first author which provided much of the funding for this project. Additional support was provided by the University of Iowa Department of Education GAANN fellowship. We want to thank Dr. Scott J. Carpenter for conducting the isotopic analyses and for providing helpful advice. Dr. Dale Leckie furnished our first samples of the Boulder Creek Formation and provided logistical assistance, meaningful discussion, and critical review of this manuscript. We also greatly appreciate the assistance of Alan Scott, and the Geological Survey of Canada. We especially want to acknowledge Dr. Paul J. McCarthy whose work has greatly influenced our methods of assessing paleosols, and who has provided stimulating discussions and advice, and critical reviews of this manuscript. Dr. Steven Driese also provided a critical review of this manuscript. Thanks also to Dr. Tim White and Dr. Art Bettis for constructive reviews of this manuscript. Thanks also to P. Lee Phillips for his assistance with core descriptions and sample collection, and Kay Saville for thin section preparation.

REFERENCES

AGRICULTURE CANADA EXPERT COMMITTEE ON SOIL SURVEY, 1987, The Canadian System of Soil Classification, 2nd Edition: Canadian Government Publishing Centre, Supply and Services Canada, Ottawa, Publication 1646.

ASHLEY, G.M., AND DRIESE, S.G., 2000, Paleopedology and paleohydrology of a volcaniclastic paleosol interval: implications for Early Pleistocene stratigraphy and paleoclimate record, Olduvai Gorge, Tanzania: Journal of Sedimentary Research, v. 70, p. 1065–1080.

BARRON, E.J., 1983, Warm equable Cretaceous, The nature of the problem: Earth-Science Reviews, v. 19, p. 305–338.

BERNER, R.A., 1981, A new classification of sedimentary environments: Journal of Sedimentary Petrology, v. 51, p. 359–365.

BESTLAND, E.A., 1997, Alluvial terraces and paleosols as indicators of early Oligocene climate change (John Day Formation, Oregon): Journal of Sedimentary Research, v. 67, p. 840–855.

BESTLAND, E.A., RETALLACK, G.J., AND SWISHER, C.C., 1997, Stepwise climate change recorded in Eocene–Oligocene paleosol sequences from Central Oregon: Journal of Geology, v. 105, p. 153–172.

BLOCH, J., 1990, Stable isotopic composition of authigenic carbonates from the Albian Harmon Member (Peace River Formation): evidence of early diagenetic processes: Bulletin of Canadian Petroleum Geology, v. 38, p. 39–52.

BREWER, R., 1964, Fabric and Mineral Analysis of Soils: New York, John Wiley & Sons, 470 p.

BULLOCK, P., FEDOROFF, N., JONGERIUS, A., STOOPS, G., TURSINA, T., AND BABEL, U., 1985, Handbook for Soil Thin Section Description: Wolverhampton, Waine Research Publications, 152 p.

CAROTHERS, W.W., LANFORD, H.A., AND ROSENBAUER, R.J., 1988, Experimental oxygen isotope fractionation between siderite-water and phosphoric acid liberated CO_2-siderite: Geochemica et Cosmochimica Acta, v. 52, p. 2445–2450.

CARPENTER, S.J., ERICKSON, M.J., LOHMANN, K.C., AND OWEN, M.R., 1988, Diagenesis of fossiliferous concretions from the Upper Cretaceous Fox Hills Formation, North Dakota: Journal of Sedimentary Petrology, v. 58, p. 706–723.

CAUDILL, M.R., DRIESE, S.G., AND MORA, C.I., 1996, Preservation of a paleo-vertisol and an estimate of Late Mississippian paleoprecipitation: Journal of Sedimentary Research, v. 66, p. 58–70.

DANSGAARD, W., 1964, Stable isotopes in precipitation: Tellus, v. 16, p. 436–468.

DETTMAN, D.L., AND LOHMAN, K.C, 2000, Oxygen isotope evidence for high-altitude snow in Laramide Rocky Mountains of North America during the Late Cretaceous and Paleogene: Geology, v. 28, p. 243–246.

DRIESE, S.G., AND FOREMAN, J.L., 1992, Paleopedology and paleoclimatic implications of Late Ordovician vertic paleosols, Juniata Formation, Southern Appalachians: Journal of Sedimentary Petrology, v. 62, p. 71–83.

DRIESE, S.G., MORA, C.I., COTTER, E., AND FOREMAN, J.L., 1992, Paleopedology and stable isotope chemistry of Late Silurian vertic paleosols, Bloomsburg Formation, Central Pennsylvania: Journal of Sedimentary Petrology, v. 62, p. 825–841.

ELICK, J.M., DRIESE, S.G., AND MORA, C.I., 1998, Very large plant and root traces from the Early to Middle Devonian: Implications for early terrestrial ecosystems and atmospheric $p(CO_2)$: Geology, v. 26, p. 143–146.

FITZPATRICK, E.A., 1984, Micromorphology of Soils: New York, Chapman & Hall, 433 p.

FRANCIS, J.E., AND FRAKES, L.A., 1993, Cretaceous climates, *in* Wright, V.P., ed., Sedimentology Review/1: London, Blackwell Scientific Publications, p. 17–30.

GAT, J.R., AND MATSUI, E., 1991, Atmospheric water balance in the Amazon Basin: an isotopic evapotranspiration model: Journal of Geophysical Research, v. 96, p. 13,179–13,188.

GLANCY, T.J., ARTHUR, M.A., BARRON, E.J., AND KAUFFMAN, E.G., 1993, A paleoclimate model for the North American Cretaceous (Cenomanian–Turonian) epicontinental sea, *in* Kauffman, E.G., and Caldwell, W.G.E., eds., Evolution of the Western Interior Basin: Geological Association of Canada, Special Paper 39, p. 219–241.

HAYS, P.D., AND GROSSMAN, E.L., 1991, Oxygen Isotopes in meteoric calcite cements as indicators of continental paleoclimate: Geology, v. 19, p. 441–444.

KRAUS, M.J., 1997, Lower Eocene alluvial paleosols: pedogenic development, stratigraphic

relationships, and paleosol/landscape associations: Palaeogeography, Palaeoclimatology, Palaeoecology, v. 129, p. 387–406.
KRAUS, M.J., 1999, Paleosols in clastic sedimentary rocks: their geologic applications: Earth-Science Reviews, v. 47, p. 41–70.
KRAUS, M.J., AND ASLAN, A., 1993, Eocene hydromorphic paleosols: significance for interpreting ancient floodplain processes: Journal of Sedimentary Petrology, v. 63, p. 453–463.
LECKIE, D.A., AND FOSCOLOS, A.E., 1986, Paleosols and Late Albian sea level fluctuations: preliminary observations from the northeastern British Columbia foothills: Geological Survey of Canada, Paper 86-1B, Current Research, Part B, p. 429–441.
LECKIE, D.A., FOX, C., AND TARNOCAI, C., 1989, Multiple paleosols of the Late Albian Boulder Creek Formation, British Columbia, Canada: Sedimentology, v. 36, p. 307–323.
LECKIE, D.A., AND REINSON, G.E., 1993, Effects of Middle to Late Albian sea-level fluctuations in the Cretaceous Interior Seaway, western Canada, *in* Caldwell, W.G.E., and Kauffman, E.G., eds., Evolution of the Western Interior Basin: Geological Association of Canada, Special Paper 39, p. 151–176.
LECKIE, D.A., AND SMITH, D.G., 1992, Regional setting, evolution, and depositional cycles of the western Canada Foreland Basin, *in* Macqueen, R.W., and Leckie, D.A. eds., Foreland Basins and Fold Belts: American Association of Petroleum Geologists, Memoir 55, p. 9–46.
LOHMANN, K.C., 1988, Geochemical patterns of meteoric diagenetic systems and their application to studies of paleokarst, *in* James, N.P., and Choquette, P.W., eds., Paleokarst: Berlin, Springer-Verlag, p. 58–80.
LUDVIGSON, G.A., GONZALEZ, L.A., METZGER, R.A., WITZKE, B.J., AND BRENNER, R.L., 1996, Diagenesis of iron minerals in the Dakota Formation, *in* Witzke, B.J., and Ludvigson, G.A., eds., Mid-Cretaceous Fluvial Deposits of the Eastern Margin, Western Interior Basin: Nishnabotna Member, Dakota Formation. A Field Guide to the Cretaceous of Guthrie County: Iowa Department of Natural Resources, Energy and Geological Resources Division, Geological Survey Bureau, Guidebook, Series no. 17, p. 31–38.
LUDVIGSON, G.A., GONZALEZ, L.A., METZGER, R.A., WITZKE, B.J., BRENNER, R.L., MURILLO, A.P., AND WHITE, T.S., 1998, Meteoric sphaerosiderite lines and their use for paleohydrology and paleoclimatology: Geology, v. 26, p. 1039–1042.
MATSUMOTO, R., AND IIJIMA, A., 1981, Origin and diagenetic evolution of Ca–Mg–Fe carbonates in some coalfields of Japan: Sedimentology, v. 28, p. 239–259.
MCCARTHY, P.J., FACCINI, U., AND PLINT, A.G., 1999b, Evolution of an ancient coastal plain: paleosols, interfluves and alluvial architecture in a sequence stratigraphic framework, Cenomanian Dunvegan Formation, NE British Columbia, Canada: Sedimentology, v. 46, p. 861–892.
MCCARTHY, P.J., MARTINI, I.P., AND LECKIE, D.A., 1997a, Pedosedimentary history and floodplain dynamics of the Lower Cretaceous upper Blairmore Group, southwestern Alberta, Canada: Canadian Journal of Earth Sciences, v. 34, p. 598–617.
MCCARTHY, P.J., MARTINI, I.P., AND LECKIE, D.A., 1997b, Anatomy and evolution of a Lower Cretaceous alluvial plain: sedimentology and paleosols in the upper Blairmore Group, southwestern Alberta, Canada: Sedimentology, v. 44, p. 197–220.
MCCARTHY, P.J., MARTINI, I.P., AND LECKIE, D.A., 1998a, Use of micromorphology for palaeoenvironmental interpretation of complex alluvial palaeosols: an example from the Mill Creek Formation (Albian), southwestern Alberta, Canada: Palaeogeography, Palaeoclimatology, Palaeoecology, v. 143, p. 87–110.
MCCARTHY, P.J., MARTINI, I.P., AND LECKIE, D.A., 1999a, Pedogenic and diagenetic influences on void coating formation in Lower Cretaceous paleosols of the Mill Creek Formation, southwestern Alberta, Canada: Geoderma, v. 87, p. 209–237.
MCCARTHY, P.J., MARTINI, I.P., AND LECKIE, D.A., 1998b, Pedogenic and diagenetic influences on void coating formation in Lower Cretaceous paleosols of the Mill Creek Formation, southwestern Alberta, Canada: Geoderma, v. 87, p. 209–237.
MCCARTHY, P.J., AND PLINT, A.G., 1998, Recognition of interfluve sequence boundaries: Integrating paleopedology and sequence stratigraphy: Geology, v. 26, no. 5, p. 387–390.
MCCARTHY, P.J., AND PLINT, A.G., 1999, Floodplain paleosols of the Cenomanian Dunvegan Formation, Alberta and British Columbia, Canada: Micromorphology, pedogenic processes, and paleoenvironmental implications, *in* Marriott, S.B. and Alexander, J., eds., Floodplains: Interdisciplinary Approaches: Geological Society of America, Special Paper 163, p. 289–310.
MORA, C.I., DRIESE, S.G., AND SEAGER, P.G., 1991, Carbon dioxide in the Paleozoic atmosphere: evidence from carbon-isotope compositions of pedogenic carbonate: Geology, v. 19, p. 1017–1020.
MOZLEY, P.S., 1989, Relation between depositional environment and the elemental composition of early diagenetic siderite: Geology, v. 17, p. 704–706.
PYE, K., DICKSON, J.A.D., SCHIAVON, N., COLEMAN, M.L., AND COX, M., 1990, Formation of siderite–Mg–calcite–iron sulphide concretions in intertidal marsh and sandflat sediments, north Norfolk, England: Sedimentology, v. 37, p. 325–343.
RETALLACK, G.J., AND MINDSZENTY, A., 1994, Well preserved Precambrian paleosols from Northwest Scotland: Journal of Sedimentary Research, v. A64, p. 264–281.
ROZANSKI, K., ARAGUAS-ARAGUAS, L., AND GONFIANTINI, R., 1993, Isotopic patterns in modern global precipitation, *in* Swart, P.K., Lohmann, K.C., McKenzie, J., and Savin, S., eds., Climate Change in Continental Isotopic Records: American Geophysical Union, Geophysical Monograph 78, p. 1–36.
SHACKLETON, N.J., AND KENNETT, J.P., 1975, Late Cenozoic oxygen and carbon isotopic changes at DSDP site 284: implications for glacial history of the Northern Hemisphere, *in* Kennett, J.P., Houtz, R.E., et al., eds., Initial Reports of the Deep Sea Drilling Project, v. 29: U.S. Government Printing Office, p. 801–807.
SMITH, D.G., AND SMITH, N.D., 1980, Sedimentation in anastomosed river systems: examples from alluvial valleys near Banff, Alberta: Journal of Sedimentary Petrology, v. 50, p. 157–164.
SPICER, R.A., AND CORFIELD, R.M., 1992, A review of terrestrial and marine climates in the Cretaceous with implications for modeling the ''Greenhouse Earth'': Geological Magazine v. 129, p. 169–180.
STELCK, C.R., AND LECKIE, D.A., 1988, Foraminiferal inventory and lithologic description of the Lower Cretaceous (Albian) Hulcross Shale, Monkman area, northeastern British Columbia: Canadian Journal of Earth Sciences, v. 25, p. 793–798.
STELCK, C.R., AND LECKIE, D.A., 1990, Biostratigraphic constraints and depositional environment of the Lower Cretaceous (Albian) Boulder Creek Formation, Monkman area, northeastern British Columbia: Canadian Journal of Earth Sciences, v. 27, p. 452–458.
UPCHURCH, G.R., JR., AND WOLFE, J.A., 1993, Cretaceous vegetation of the Western Interior and adjacent regions of North America, *in* Caldwell, W.G.E., and Kauffman, E.G., eds., Evolution of the Western Interior Basin: Geological Association of Canada, Special Paper 39, p. 243–281.
WHITE, T.S., GONZÁLEZ, L.A., LUDVIGSON, G.A., AND POULSEN, C., 2001, The mid-Cretaceous greenhouse hydrologic cycle of North America: Geology, v. 29, p. 363–366.
WRIGHT, V.P., 1986, Pyrite formation and the drowning of a palaeosol: Geological Journal, v. 21, p. 139–149.
WRIGHT, V.P., 1994, Paleosols in shallow marine carbonate sequences: Earth-Science Reviews, v. 35, p. 367–395.

Received 12 December 2000; accepted 26 April 2001.